JPMTR 129 | 1911
DOI 10.14622/JPMTR-1911
UDC 676.2:621.5:531.2(182)

Original scientific paper
Received: 2019-10-28
Accepted: 2020-03-25

Compressive stress–strain behavior of paper material affected by the actual contact area

Jian Chen[1], Edgar Dörsam[2], Jann Neumann[3] and Simon Weißenseel[2]

[1] School of Mechanical Engineering, Yangzhou University, Huayang Weststr. 196, 225127 Yangzhou, China
[2] Institute of Printing Science and Technology, Darmstadt University of Technology, Magdalenenstr. 2, 64289 Darmstadt, Germany
[3] Perfecta Cutting Systems GmbH, Schäfferstr. 44, 02625 Bautzen, Germany

chenjian.tud@hotmail.com
doersam@idd.tu-darmstadt.de
neumann@perfecta.de
Simon.Weissenseel@alcon.com

Abstract

The surface topography plays a very important role in the mechanical behavior of paper materials, especially for the compressive properties of thin sheet. When the surface of the cylindrical indenter is very smooth, the actual contact area under force is usually much smaller than the nominal contact area because of the surface roughness of the paper. This paper shows a method for measuring the actual contact area; with the aid of a microscope, a new approach based on image processing technique is presented to calculate the relationship between force and actual contact area. With the help of this method, the actual pressure–deformation relation and the actual modulus of paper could also be calculated. The calculation results show that there is an obvious difference between the results calculated by actual and nominal contact area. The varied trend and the values of the actual modulus are also obtained; at the beginning of the loading the actual modulus is decreasing and then close to a constant value. The universal testing machine Zwick Z050 and the optical surface topography measuring machine Sensofar Plu Neox were employed to determine not only the strength and deformation performance but also the surface roughness of specimen. Based on the obtained results the influence of carbon paper on the compressive behavior of copy paper is further discussed from different standpoints. The numerical results demonstrate the feasibility and effectiveness of the new method.

Keywords: carbon paper, copy paper, stress–strain curve, compression modulus, surface topography

1. Introduction and background

The surface topography of paper is responsible for many important paper properties, such as gloss, and printability. The measurement and characterization of the paper's surface structure is a very important task. There are many components that are used in the paper-making process. The interactions between these components are responsible for creating the properties of the paper. The paper's surface topography can range from very rough to extremely smooth, which obviously also has an influence on mechanical properties of paper materials, especially the compressive behavior.

Generally, the surface topography is rated by using smoothness or roughness (Pino and Pladellorens, 2009). Roughness plays an important role in determining how a real object will interact with its environment. A roughness value can either be calculated on a profile (line) or on a surface (area). For the profile roughness, the average roughness R_a is the most widely used parameter. For areal roughness parameters, the average areal roughness, S_a, is more common.

The measurement and characterization of surface roughness are very important not only for paper materials, but also for metal or other materials. For example, Buchner (2008, p. 118) presented a new method for evaluating the relationship between the real contact area and the normal load. The relative real contact area of an aluminum sheet under force was calculated. In the presented papers of Chen, et al. (2013; 2014), the effect of surface roughness on the nanoindentation measurements was investigated by using finite element method; the material AISI 316 L stainless steel was used in the simulation and a 3D model with seven levels of surface roughness was developed to simulate the load-displacement behavior in an indentation process.

For paper materials, the influence of surface roughness on the compressive behavior of different papers was studied by Rättö (2005), who pointed out that when compressing thin sheets, it was important to be aware of the influence of surface roughness. In the model proposed by Schaffrath and Göttsching (1991; 1992a; 1992b), the paper body was described as one internal structure and two rough surfaces, the surface topography was described as pyramid elements, and the force–deformation relationship of paper materials was derived by using the Newton formula. A new mathematical model of paper structure and paper–press interactions was introduced by Provatas and Uesaka (2003), where the effects of fiber furnish on surface structure were examined, and the factors controlling the paper–plate contact during printing were investigated. In addition, the modification of the micro-structure at various scales of the paper surface due to the calendering process was described (Vernhes, et al., 2009; Vernhes, Dubé and Bloch, 2010).

Most other studies of paper surface roughness are still focused on experimental aspects. A number of techniques are available for characterizing the topographical features of paper surfaces; four different methods were evaluated for characterizing the smoothness of the handsheet (Singh, 2008). A fast photometric stereo method, used for the determination of surface topography and reflectance was proposed (Hansson and Johansson, 2000), and the paper surface topography under compression was also studied (Teleman, et al., 2004). Furthermore, the surface topographical differences between cross machine and machine direction for the newspaper and paperboard were investigated (Alam, et al., 2011).

Preload is often used in testing a specimen, for a process when the crosshead moves to load the specimen to a specified value before a test starts. The use of preload can improve the accuracy and repeatability of results, because the initial contact area of the surface structure is not changed from zero.

According to the metrology definitions, surfaces are classified as three groups: nominal surface, actual (real) surface and measured surface. Nominal surface is the ideal surface defined by the design, and in practice this surface does not exist; actual surface is the real physical surface that limits the body; measured surface is the surface obtained by any measurement system. Normally, the stress–strain relations of most of the materials are calculated by using the nominal contact area. The difference between actual and nominal contact area is thus ignored, while actually, for contact surface, the nominal contact area A_0 and the actual contact area $A(z)$ should be very different. Therefore, not in all the situations can be neglected. The schematic diagram of the difference between nominal and actual contact areas is shown in Figure 1.

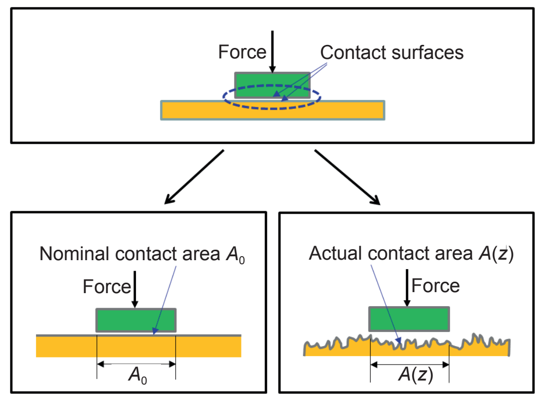

Figure 1: Schematic diagram of the difference between nominal and actual contact areas

Generally, when the indenter is very smooth, the actual contact area is much smaller than the nominal contact area because of the roughness of the paper surface. In this paper, a new experimental method for evaluating the relationship between the actual contact area and the normal load is proposed. A carbon paper is introduced in this method, and it is assumed that the measured contact areas between carbon paper and copy paper are regarded as the actual contact areas between the indenter and copy paper. Based on this assumption, the mechanical behavior of paper in through-thickness direction is discussed by deducing the actual modulus and calculating the actual stress–strain relation. Finally, the influence of the carbon paper is discussed from various aspects.

2. Materials and Methods

The copy paper (DIN A4, 80 g/m^2) selected for doing the research is produced by the Steinbeis Paper GmbH. The actual average thickness is d = 84.7 µm.

2.1 Pressure-sensitive materials

The material used here to show the contact area is carbon paper. In this research, the carbon paper Geha-1 (DIN A4, 29 g/m^2), which is produced by Geha Werke Hannover was firstly used to introduce the experimental process. The average thickness of the carbon paper Geha-1 is d = 43.6 µm. The force sensitivities of seven other different types of carbon papers were compared: SH carbon papers (SH-1, SH-2 and SH-3) produced by Shanghai Huideli Co., Ltd., DL carbon papers (DL-1, DL-2 and DL-3) produced by Deli Group Co., Ltd., and anotther carbon paper produced by Geha Werke Hannover (Geha-2), see section 3.2. The SH-1 carbon paper was selected to obtain more precise results.

Some other materials such as Fujifilm's pressure measuring film (Fujifilm, 2016) can be used to show the actual contact areas (Bachus, et al., 2006). These films can also be used for measuring the distribution of pressure (Luong, 1999, p. 66; Endres, 2006, p. 56). But in this research, Fujifilm's pressure sensitive films were not selected for measuring the distribution of pressure on copy papers, mainly because of the following two reasons.

Firstly, the Fujifilm product which can be used for measuring the low pressure is two-sheet type, which means two films (A-Film and C-Film) should be used at the same time. The maximum force used in this study was 100 N, and the contact area was around 28.27 mm^2; the ideal contact pressure thus was around 3.54 MPa, for which another type of film is suitable. On the other hand, for the very small force, for example 2 N, the pressure was only about 0.07 MPa. To keep the uniformity and correctness of the results, we cannot use three different types of films in the same test.

Secondly, considering the smaller thickness of copy paper and the surface roughness of the A-Film and C-Film, these kinds of films are not suitable to be used for the experiments described in this paper.

In the research of Endres (2006), a new pressure-sensitive film (STFI film) was developed to show the pressure distribution on the sample surface. On the one hand, the STFI film can be used for measuring the pressure range from 1 MPa to 50 MPa, but unfortunately, this film is not enough sensitive when the pressure is smaller than 1 MPa. The highest pressure used in this research was about 3 MPa, and with such a small pressure, this STFI film cannot be used to show the contact area clearly. On the other hand, the same problem as with the Fujifilm is present: the thickness of this film is 128 µm, which is more than the thickness of copy paper (84.7 µm), which would lead to big errors of the measurements.

2.2 Experimental setup

To eliminate the effect of climate conditions of the environment on the mechanical force–deformation behavior, the experimental studies were performed under standardized climatic conditions. The climate is specified in DIN 50014 and prescribed in a range of 23 ± 0.5 °C for the temperature and in a range of 50 ± 1.5 % for the relative humidity (Deutsche Institut für Normung, 2018). The samples were preliminarily treated according to DIN EN 20187 (Deutsche Institut für Normung, 1993) in order to assure an equal moisture condition in the various items delivered (Kaulitz and Dörsam, 2008).

The loading process was conducted on ZWICK Z050, which could be utilized for strain, shear and bending tests with different substrates and machine components with high accuracy of the cross head speed (0.0005–2 000 mm/min), position repetition accuracy (± 2 µm), and drive system's travel resolution (27 nm) (Kaulitz and Dörsam, 2008; Kaulitz, 2009, p. 179). The measurement device was equipped with travel sensor Heidenhain-Metro MT 2581, with the resolution of 50 nm and the repetition accuracy of 0.2 µm (Kaulitz, 2009, p. 179), produced by HEIDENHAIN GmbH. The structure of the compression device in ZWICK machine is shown in Figure 2.

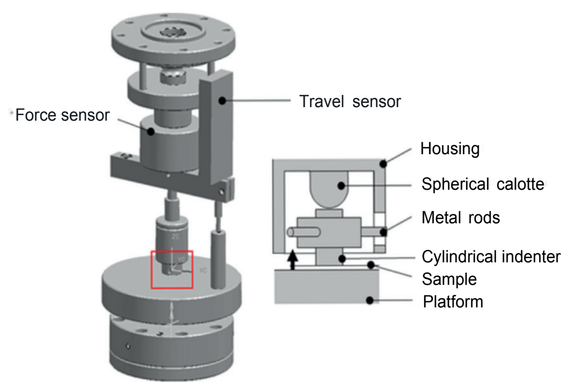

Figure 2: Test device for measuring the compressive force deformation behavior of paper (Kaulitz, 2009, p. 179)

In the device shown in Figure 2, the diameter of the cylindrical indenter is 6 mm, the area of the indenter A_{ind} is shown in Figure 3. The areal roughness of the indenter and platform could be measured by using the Sensofar PLu Neox profilometer with the objective EPI 10X-N in confocal profiling mode. The areal roughness of the indenter S_{ind} is about 385 nm and the areal roughness of the platform S_{pla} is around 650 nm. Compared with the areal roughness of paper, the S_{ind} and S_{pla} are really very small, therefore the influence from the surface roughness of indenter and platform could be ignored.

The setup of this experiment is shown in Figure 3. In order to show the actual contact areas between the indenter and copy paper, a carbon paper (Geha-1) was put above the copy paper. For carbon paper, which has two sides, only one side is the ink side; the ink side should directly be in contact with the copy paper and then the load can be imposed on the other side of carbon paper. When the force was removed, the ink of the carbon paper would be transferred on the surface of copy paper. In the following calculations, the actual contact areas between the indenter and copy paper were replaced by the measured contact areas between carbon paper and copy paper.

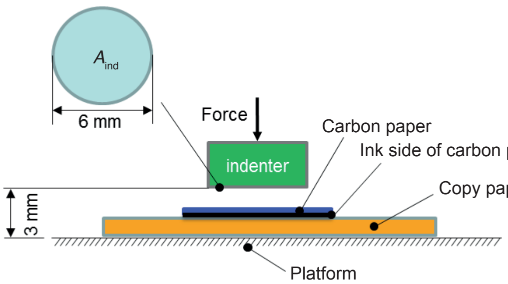

Figure 3: Experimental setup used for measuring the actual contact area

At the beginning of the loading process, the indenter moves down at the speed of 20 mm/min, until the indenter comes into contact with the surface of the carbon paper. The preload here was set as 1 N; when the change of force is 1 N, the compression process will begin at the speed of 0.05 mm/min. When the force reaches the desired maximum force, the indenter moves up at the speed of 0.05 mm/min. When the force decreases to 1 N, the indenter returns back to the original position at the speed of 20 mm/min.

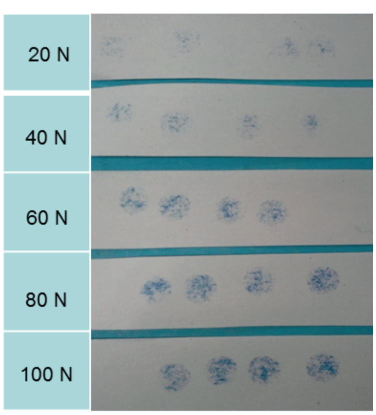

Figure 4: Measured contact areas between the carbon paper and copy paper under different forces

Five groups of preliminary experiments were carried out, the results of which are shown in Figure 4. The forces applied were 20 N, 40 N, 60 N, 80 N and 100 N. It is obvious that different forces lead to different contact areas. To improve the accuracy of the method, the force imposed in the main experiment was changing from 0 N to 100 N, with the substep of 2 N, which means 50 groups of measurements (2 N, 4 N, 6 N, 8 N,..., 96 N, 98 N, 100 N) were implemented; for each group, 20 tests were finished.

2.3 Enlarging and transferring pictures

The image processing technique was used to separate the contact area from the background. The surface of the specimen was magnified 25 times under binocular microscope and captured by a camera with resolution of 1200 × 1600 pixels. Then by the aid of MATLAB 8.1, all pictures were transformed to binary images (MATLAB help, 2013), as shown in Figure 5.

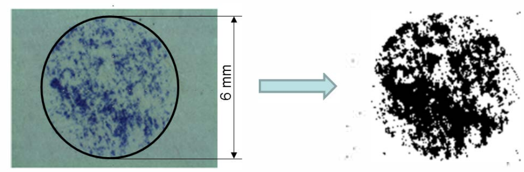

Figure 5: The example of original and binary picture

Binary images are often produced by thresholding a greyscale or color image, in order to separate an object in the image from the background. The color of the object is referred as the foreground color. The rest is referred to as the background color. MATLAB provides some methods to transform an original picture to a binary picture. The key problem here is how to determine the threshold value, as the final result is directly determined by this value. Figure 6 shows an example of the calculation results by using different threshold values. The threshold values applied here are 0.5, 0.25 and calculated by the Otsu method (Otsu, 1979). The three transformed figures are significantly different compared to the original picture, but the result of the Otsu method is the closest to the original picture (see Figure 6).

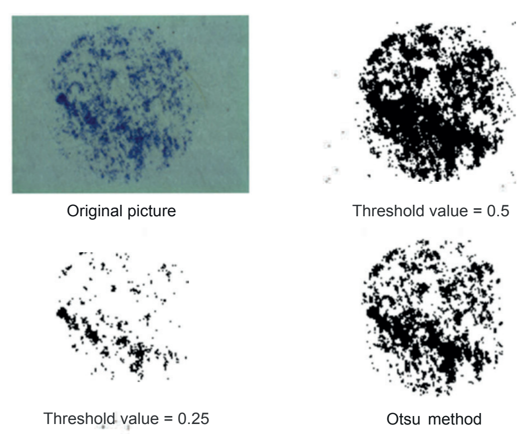

Figure 6: Examples of allpying different threshold values in transformation to a binary image

Otsu method (Otsu, 1979), named after its inventor Nobuyuki Otsu, is one of the most popular binarization algorithms. In computer vision and image processing, Otsu method is used to automatically perform clustering-based image thresholding or reduction of a gray level image to a binary image.

2.4 Calculating the contact area

For different pictures, the Otsu method will produce different threshold values. The average threshold value was calculated and used to obtain the binary images. For each of the five groups of preliminary experiments (20 N, 40 N, 60 N, 80 N, 100 N), four tests were finished (see Figure 7).

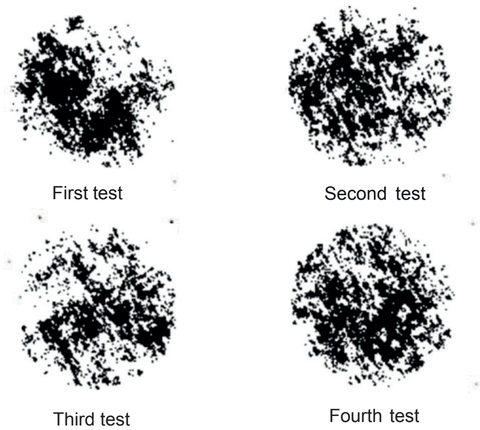

Figure 7: Example of binary images for one set of tests (Average threshold value = 0.4514, force = 100 N)

The binary pictures have resolution of 1200 × 1600 pixels, which is the same as the original pictures. The number of the pixels that belong to the black area can be calculated by using the ‘‘bwarea’’ command (MATLAB help, 2013) in MATLAB. Then, according to the proportional relation between the pixels of black area and the whole area, the value of the black area can be calculated, which is the measured contact area A_{mea}, in this paper regarded as equivalent to the actual contact area $A(z)$.

2.5 Calculating the force–contact area relation

The experiments described in section 2.2 were performed under some discrete forces. When the changes of these forces are very small, it is reasonable to assume that the deformation behavior of the material under small forces accord with the theory of elasticity. Hooke’s law is the law of elasticity E under small deformation, stating that, for relatively small deformations of an object, the displacement or the size of the deformation is directly proportional to the deforming force or load. Hooke’s law (Equation [1]) can also be expressed in terms of stress (σ) and strain (ε). According to Hooke’s Law:

$$\sigma = \frac{E \cdot A_0}{l_0} \cdot z = E \cdot \varepsilon \Leftrightarrow F \qquad [1]$$

where A_0 is the nominal contact area, l_0 is the original length or thickness of the material, and z is the deformation under the force F.

For paper structure, the force–deformation relation can be expressed as follows:

$$F(z) = \frac{E(z) \cdot A(z)}{d} \cdot z \qquad [2]$$

with $E(z)$ being the actual modulus, which is changing with the discrete force $F(z)$, and $A(z)$ being the actual contact area, which is the discrete area calculated by the method described above, and d being the original thickness of paper.

The actual modulus of paper under different forces could be expressed as the product of actual contact pressure, paper thickness and the inverse of the total deformation.

$$E(z) = \frac{F(z)}{A(z)} \cdot \frac{1}{z} \cdot d = W(z) \cdot \frac{1}{z} \cdot d \qquad [3]$$

where:

$$W(z) = \frac{F(z)}{A(z)} \qquad [4]$$

is the actual contact pressure.

All the variable values needed here could be obtained from the implemented experiments. This method can only be used for small deformation under discrete forces.

3. Results

In this part, a simple method by using the Geha-1 carbon paper is firstly introduced to show the contact areas. Then, after comparing the sensitivities of dif-

Table 1: Experimental results of the measured contact areas under different forces with Geha-1 carbon paper

Force (N)	First test (mm^2)	Second test (mm^2)	Third test (mm^2)	Fourth test (mm^2)	Average (mm^2)	Standard deviation (mm^2)
20	3.277	3.545	3.545	3.214	3.395	0.003
40	5.811	5.885	5.503	4.521	5.430	0.011
60	9.601	10.475	9.527	9.013	9.654	0.011
80	10.269	11.508	9.379	12.610	10.941	0.025
100	10.909	13.015	12.621	13.209	12.438	0.018

ferent carbon papers as well as Fujifilm materials, a more precise method by using the SH-1 carbon paper is implemented to show the contact areas.

3.1 Preliminary calculation of the stress–strain curve of paper

In the preliminary experiments, the measured contact areas under different forces (20 N, 40 N, 60 N, 80 N, 100 N) were calculated. The results of the measured contact areas with standard deviation are shown in Table 1 and Figure 8.

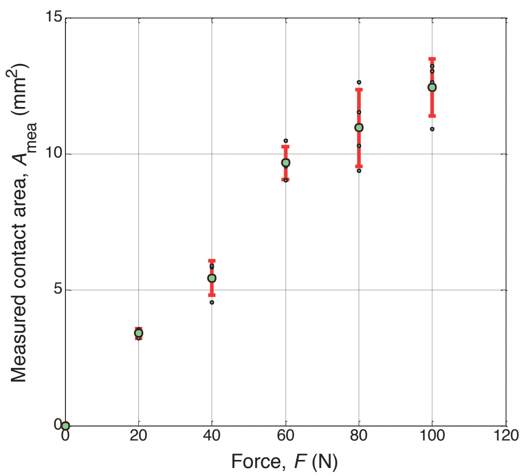

Figure 8: Measured contact areas under different forces with Geha-1 carbon paper; the error bar represents the average (mean) value and the standard deviation

The average values of each group are also plotted in Figure 9 as the discrete points. Then, the values of measured contact areas under other forces can be calculated by using the quadratic curve fitting method.

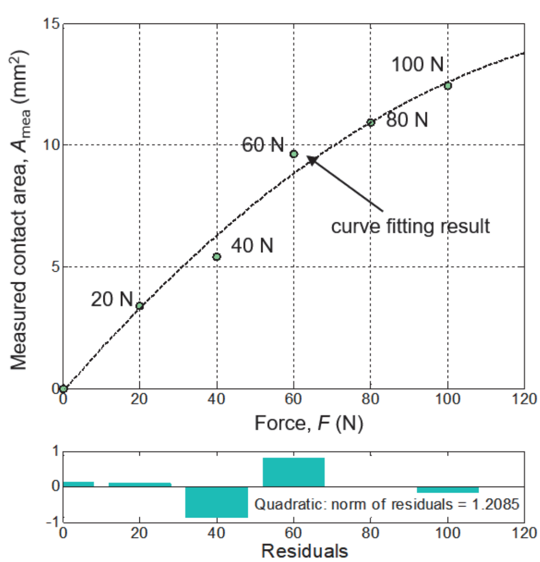

Figure 9: Measured contact areas under different forces with Geha-1 carbon paper, with quadratic curve

In Figure 9, the quadratic curve fitting method was used in the first graph. The second graph shows the corresponding residuals. The dashed black line is the fitting curve of these discrete values. The fitting function is provided as Equation [5].

$$A_{med} = 5.56 \cdot 10^{-4} \cdot F^2 + 0.183 \cdot F - 0.127 \qquad [5]$$

For this curve fitting function, the norm of residuals is equal to 1.209 and the coefficient of determination is R^2 = 0.988. The calculation results show that this method can be well used to calculate the measured (actual) contact area A_{mea} ($A(z)$) under different forces $F(z)$, as well as the relationship between force and actual contact area.

According to Equation [4] and the calculation results obtained in Figure 9, the actual pressure $W(z)$ can be calculated. The values are listed in Table 2.

Table 2: Experimental (z, A) and calculation (W) results of the deformation, contact area, and actual pressure for Geha-1 carbon paper

$F(z)$(N)	0	20	40	60	80	100
z (µm)	0	3.66	5.68	7.26	8.62	9.78
$A(z)$ (mm²)	0	3.40	5.43	9.65	10.94	12.44
$W(z)$ (N·mm⁻²)	0	5.89	7.37	6.22	7.31	8.04

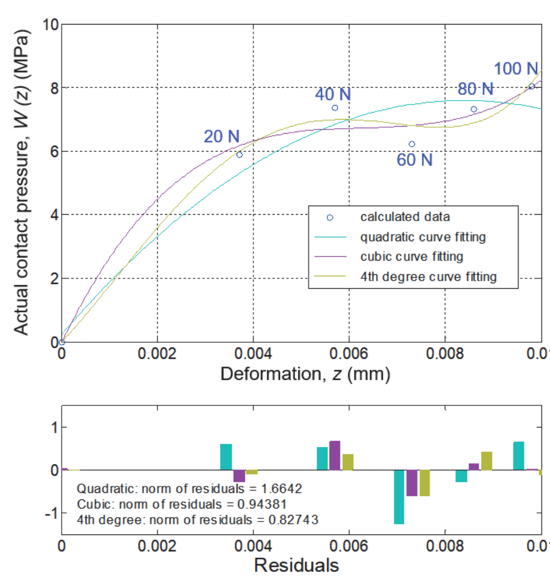

Figure 10: Relationship between the actual contact pressure and the deformation of copy paper for Geha-1 carbon paper

Here some discrete contact pressure values under different forces were obtained. The values of force $F(z)$ and the deformation z were directly obtained by Zwick machine. The values of the actual contact area $A(z)$

and the actual contact pressure $W(z)$ were obtained by the new experimental method and Equation [4]. With the method of curve fitting, the relationship between actual contact pressure $W(z)$ and deformation z was calculated and shown in Figure 10.

Three different curve fitting methods were used, the functions of which are provided in Equation [6].

Quadratic curve fitting:

$$W(z) = -0.105 \cdot z^2 + 1.76 \cdot z + 0.243 \qquad [6]$$

Cubic curve fitting:

$$W(z) = 0.0265 \cdot z^3 - 0.499 \cdot z^2 + 3.16 \cdot z - 0.029$$

4th degree curve fitting:

$$W(z) = 5.22 \cdot 10^{-3} \cdot z^4 - 0.0829 \cdot z^3 + 0.227 \cdot z^2 + 1.66 \cdot z - 6.41 \cdot 10^{-3}$$

Comparisons of corresponding residuals between different curve fitting methods are shown in the second part of Figure 8, which are used to see whether the lines are good fit for the discrete data. Both the quadratic (R^2 = 0.936), cubic (R^2 = 0.980) and 4th degree (R^2 = 0.985) curve fitting methods could be used for describing the trend of the calculated data. The residual values of cubic and 4th degree curve fitting are much smaller than the quadratic curve fitting. From the view of physical properties, no matter by using which kinds of curve fitting methods, the stress-strain–curve of paper with considering the surface roughness is very similar to the general elastic-plastic materials (Tournier, 2003). Further in this paper, cubic curve fitting method was chosen for describing the actual stress–strain curve.

When the force is changing from 0 N to 20 N, the deformation of the paper is nearly 4 μm; when the force is changing from 20 N to 100 N, the deformation of paper is only 6 μm. At the beginning of the contact, a small change in force leads to a large change in deformation. Compared with the internal structure with hard fibers, the surface structure of the paper is much easier to be compressed. When the thickness of the paper is very thin, the influence of surface roughness on the compressive response is very important and cannot be neglected.

According to Equation [3] and Table 2, the actual modulus $E(z)$ of paper under different forces can be calculated, by using the quadratic curve fitting method (see Equation [7]). The numerical trend can be described. Figure 11 shows the relationship between the actual modulus and the strain. The blue curve is the corresponding curve fitting result (see Equation [7]), R^2 = 0.954. When the force is changing from 20 N to 100 N, the actual modulus of paper is decreasing from 136 MPa to around 70 MPa.

$$E(z) = 1.77 \cdot 10^6 \cdot z^2 - 3.53 \cdot 10^4 \cdot z + 244.6 \qquad [7]$$
$$z = 0.0847 \cdot \varepsilon$$

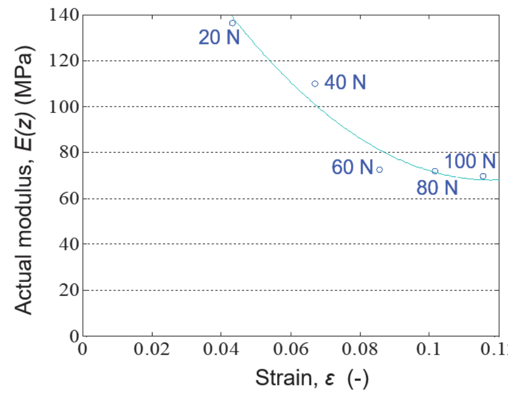

Figure 11: Stress–strain relationship of copy paper

Generally, the behavior of paper in the in-plane direction could be regarded as the elastic-plastic behavior (Xia, Boyce and Parks, 2002). But the modulus of paper material in the out-of-plane is not a constant value, which cannot be simply described by using the E-modulus (Mark, et al., 2001). The modulus of wood materials is considered to range from about 10 MPa to 25 GPa (Drexler, 2009); unfortunately, only very few researches discussed the modulus of paper in the out-of-plane direction. The modulus of paper in the in-plane direction is much bigger than the modulus in the out-of-plane direction. For example, the E-modulus of paperboard provided by Xia, Boyce and Parks (2002) in machine direction is about 5.6 GPa, and in cross machine direction is about 2.0 GPa, while the initial modulus in the out-of-plane direction is 18 MPa. The initial E-modulus of another paperboard in the out-of-plane measured by Stenberg (2003) is 34 MPa, and the E-modulus of this paperboard for fully compacted solid is about 5 GPa.

Based on the above findings, it can be seen that the calculation results of the actual modulus are reasonable. At the beginning of the compression process, the actual modulus of paper is decreasing because of the surface roughness, with the contact area approaching to the maximum contact area (approximately equal to the nominal contact area A_0), the actual modulus will be decreased to a constant value.

Figure 12 unfolds a clear comparison between the stress–strain curves of paper calculated by different methods. The compressive behavior of paper under actual contact area is very different from the result calculated by using the nominal contact area.

For the actual stress–strain curve, at the beginning of the loading process, the stiffness of paper increases with the increasing load and the relationship between stress and strain is nearly linear (or very close to linear), especially when the force is smaller than 20 N, but after that the stiffness decreases with increasing load, which is very similar to other elastic-plastic materials. For the nominal stress–strain curve, the loading process shows a typical J-shaped curve. The calculation method of the contact area plays a very important role.

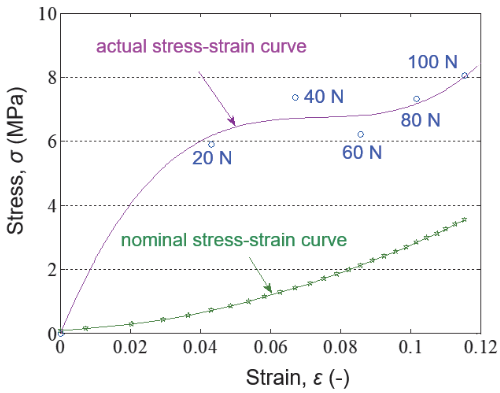

Figure 12: Compressive stress–strain curves of copy paper calculated by using the actual contact areas (red curve) and the nominal contact areas (green curve)

3.2 A more accurate method for calculating the stress–strain curve

As mentioned before, the carbon paper used for preliminary experiments was Geha-1. When the applied force is smaller than 20 N, this type of carbon paper is not sensitive enough to show the contact area. Figure 13 shows the force sensitivity of carbon paper Geha-1, for four different forces imposed on the surface of carbon paper. It can be seen that the contact area is not clear anymore when the force is smaller than 20 N. To improve the accuracy of the calculation results, some other tests should be implemented. It is better to find a much more sensitive material, to show the actual contact areas.

Seven other different types of carbon papers (SH-1, SH-2, SH-3, DL-1, DL-2, DL-3, Geha-2) from three different companies were selected. Two types of Fujifilm (Fuji-LLW and Fuji-LLLW) were also tested here. For each of the carbon papers, four different forces (2 N, 10 N, 20 N, and 100 N) were imposed on the materials.

It can be seen from Figure 14 that the sensitivities of different carbon papers are quite different; only SH-1, Geha-2 and Fuji-LLLW can be used for measuring low pressure. The sensitivity of SH-1 is very close to the sensitivity of Fuji-LLLW. When the force is smaller than 10 N, the contact areas can also be shown on the copy paper. The SH-1 carbon paper was selected in the following experiment for showing the contact areas under different forces.

The experimental process was reorganized as given in Section 2.2 and 50 groups of experiments were implemented. An example of contact area measurement is shown in Figure 15. The evaluation method was the same as before: all the pictures were transformed to the binary images and then the contact areas could be calculated. The calculated results are shown in Figure 16, where each point represents the average contact area of 20 tests under the same force.

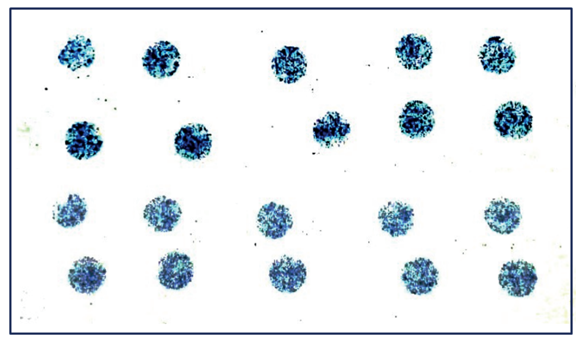

Figure 15: Example of measured contact areas (the force here is 90 N)

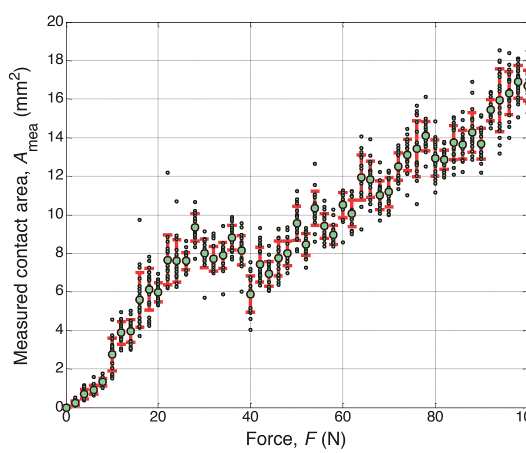

Figure 16: Measured contact areas for copy paper with SH-1 carbon paper under forces changed in steps of 2 N

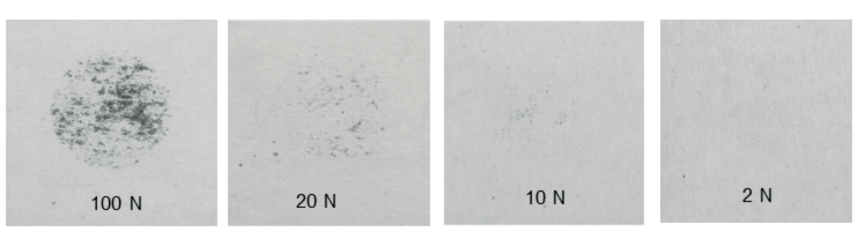

Figure 13: Sensitivity tests of carbon paper (Geha-1)

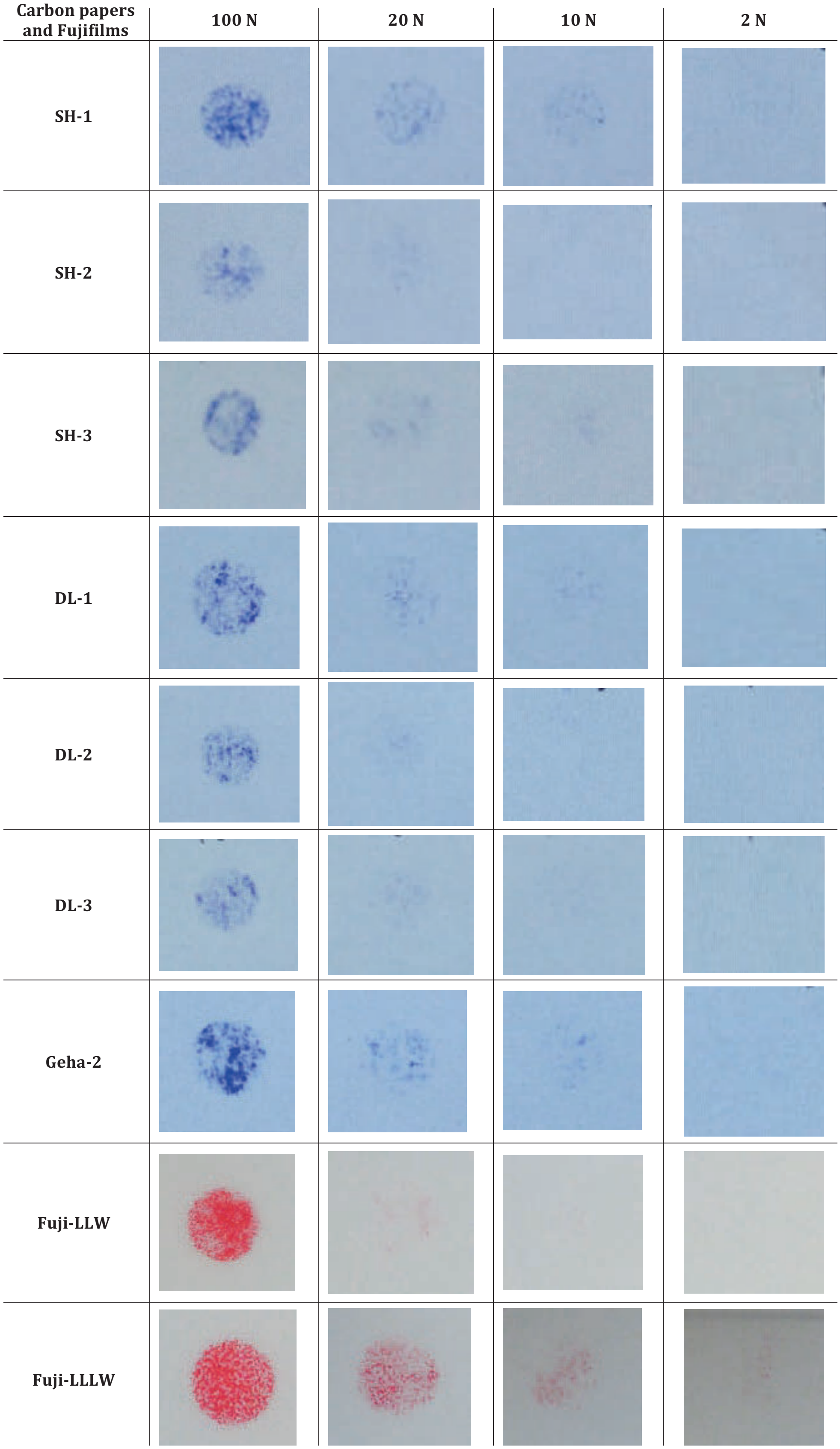

Figure 14: Sensitivity tests of seven different carbon papers and two Fuji-films

The average values of the measured contact areas under different forces were plotted in Figure 17 as discrete points. The relationship between the measured contact area A_{mea} and force F can be drawn by the curve fitting method. The cubic curve fitting method was used here; the fitting function is provided as follows:

$$A_{mea} = 3.6 \cdot 10^{-5} \cdot F^3 - 0.0057 \cdot F^2 + 0.39 \cdot F - 0.24 \qquad [8]$$

The calculation result (R^2 = 0.953) shows that this method can be well used to calculate the measured (actual) contact area A_{mea} ($A(z)$) under different forces $F(z)$.

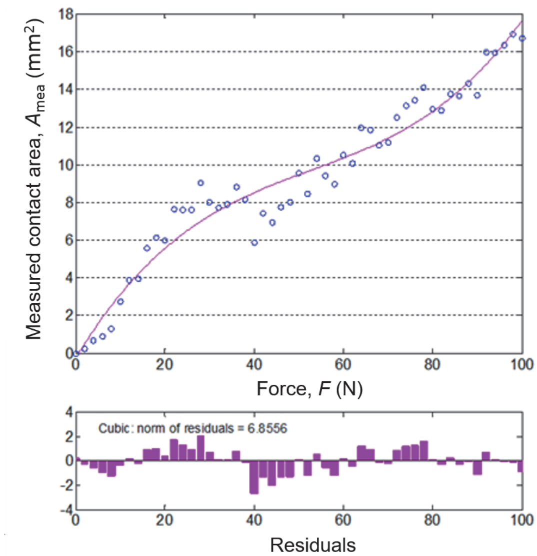

Figure 17: Measured contact areas for copy paper with SH-1 carbon paper under different forces with cubic curve fitting

By using this new method, we can redraw the actual modulus–strain curve (see Figure 18) and the actual stress–strain curve (see Figure 19).

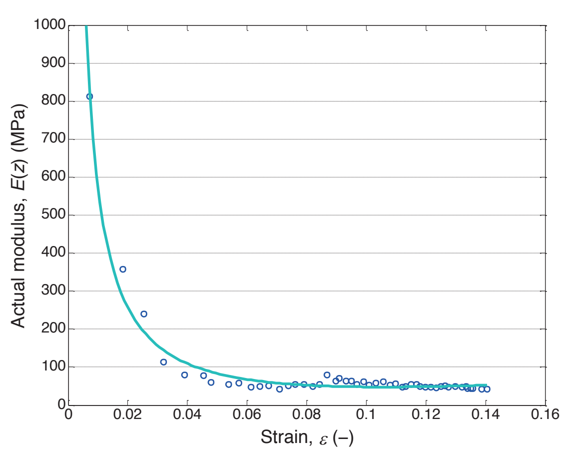

Figure 18: Relationship between the actual modulus and strain for copy paper with SH-1 carbon paper

Figure 18 shows the relationship between the actual modulus and the strain (or deformation). The discrete data were calculated according to Equation [3]. The blue curve is the corresponding curve fitting result (Equation [9]), R^2 = 0.977.

$$E(z) = -72.73 + 6730.15 \cdot z + 0.54 \cdot \frac{1}{z} \qquad [9]$$
$$z = 0.0847 \cdot \varepsilon$$

When the force is changed from 2 N to 100 N, the actual modulus of paper will decrease from 812 MPa to around 50 MPa. As mentioned before, at the beginning of the compression process, the actual modulus of paper is very big which is mainly because the actual contact area is very small. When the contact area approaches to the maximum contact area, the actual modulus will be decreased to a constant value.

According to Equations [4] and [8], the actual stress–strain curve of paper can also be recalculated. The new actual stress–strain curve is shown in Figure 19.

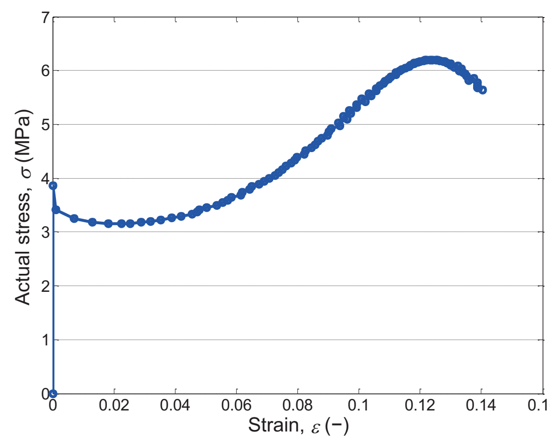

Figure 19: Compressive stress–strain curve of copy paper calculated by using the actual contact areas with SH-1 carbon paper

From Figure 19, we can reasonably infer that the surface topography has a considerable influence on the compressive behavior of paper materials.

When the surface roughness is taken into account, the stress–strain curve of paper material is not typically J-shaped anymore.

4. Discussion

Based on the results obtained in section 3, we can see that by considering the surface roughness, the stress–strain curve of paper material is more like that of a typical elastic-plastic material (see Figure 20). Many engineering materials show this kind of behavior, such as steels used for automotive seat structure (Yuce, et al., 2014), polymers with strain hardening behavior (Senden, 2013, p. 119), aluminum alloy and steel plates tested in laboratory (Liu, Villavicencio and Soares, 2013), and so on.

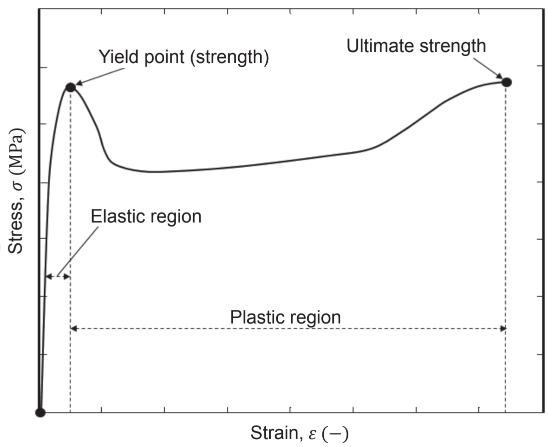

Figure 20: Typical stress–strain curve of an elastic-plastic material, adopted from Turner and Burr (1993)

As shown in Figure 20, some typical characteristics used for determining the elastic-plastic material, for example, the plastic region, the yield strength and the ultimate strength, etc., all of these behaviors can also be found in Figure 19.

The elastic region of paper material is relatively small, which means the behavior of paper material is more close to perfectly plastic materials.

Although, in most situations, the mechanical behavior of paper material is regarded as J-shaped. But it can be seen from the work done in this research that, in essence, paper is still an elastic-plastic material. The surface roughness plays a very important role in presenting the mechanical behavior.

In addition, for the compression behavior of paper material, the obtained stress–strain curve after ultimate stress is decreasing, rather than increasing, which may be caused by the change of the internal structure or by the selected curve fitting function (see Figure 17).

5. Conclusions

First of all, two important concepts were presented in this paper: the actual compression modulus and the actual stress–strain curve of paper. Paper is not a linearly elastic material. The elastic modulus (E-modulus) of a material with non-linear elastic stress–strain response was defined as the slope of the tangent line to the stress–strain curve at the origin and therefore depends only on the small strain behavior. Because of the long experience with linearly elastic metals, the idea of an E-modulus was carried over to paper, but the physical meaning of such a modulus for paper is not clear (Mark, et al., 2001). In this paper, the concept of actual modulus is presented. The actual compression modulus of paper is not a constant value, which was also calculated. Then, nearly all research works presented up to now discussed the stress–strain curve of paper by using the nominal contact area. But actually, the stress–strain curve of paper is apparently affected by the surface topography. So the concept of actual stress–strain curve was introduced here to study the mechanical behavior of paper materials.

In addition, a new experimental method was proposed to calculate the actual contact areas. Its calculation results identified the practicability of the method. Different types of carbon papers have been selected and compared. With the help of actual contact areas obtained, the actual compression modulus and the actual stress–strain curve of copy paper were calculated. The calculation results show the crucial differences between the actual and nominal stress–strain behaviors.

In summary, according to the presented research results, the stress–strain curve of paper calculated by using the actual contact area is totally different from the calculation result of the nominal contact area. The mechanical behavior of paper materials under compressing by considering the surface roughness is very close to the general elastic-plastic materials. The influence of the surface roughness cannot be ignored and special attention should be given to the research of the paper surface topography.

Acknowledgements

The authors gratefully acknowledge the financial support from the Jiangsu Science and Technology Department (Project Number: BK20190873). All experiments mentioned in this paper were implemented by using the testing machine ZWICK Z050 in IDD (Institute of Printing Science and Technology, Technische Universität Darmstadt).

List of Abbreviations

A_0	Nominal contact area
A_{ind}	Nominal area of the indenter, which is equal to the value of the nominal contact area A_0
A_{mea}	Measured contact area, which is regarded as equivalent to the actual contact area $A(z)$
$A(z)$	Actual contact area, which is changing with deformation z
d	Original thickness of the paper (d = 0.0847 mm)
E	E-modulus, which is a constant value
$E(z)$	Actual modulus, which is changing with deformation
F	Force
$F(z)$	Force when the deformation is z
l_0	Original length or thickness of the material
R_{a}	Average profile roughness
S_{a}	Average areal roughness
S_{ind}	Average areal roughness of the indenter
S_{pla}	Average areal roughness of the platform
$W(z)$	Actual contact pressure
z	Deformation of paper in the out-of-plane direction
ε	Strain
σ	Stress

References

Alam, A., Thim, J., Manuiskiy, A., O'Nils, M., Westerlind, C., Lindgren, J. and Lidén, J., 2011. Investigation of the surface topographical differences between the Cross Direction and the Machine Direction for newspaper and paperboard. *Nordic Pulp & Paper Research Journal*, 26(4), pp. 468–475. https://doi.org/10.3183/npprj-2011-26-04-p468-475.

Bachus, K.N., DeMarco, A.L., Judd, K.T., Horwitz, D.S. and Brodke, D.S., 2006. Measuring contact area, force, and pressure for bioengineering applications: using Fuji Film and TekScan systems. *Medical Engineering & Physics*, 28(5), pp. 483–488. https://doi.org/10.1016/j.medengphy.2005.07.022.

Buchner, B., 2008. *Investigation of friction in closed-die warm forging of aluminium alloys*. Doctoral thesis. University of Leoben.

Chen, L., Ahadi, A., Zhou, J. and Ståhl, J., 2013. Modeling effect of surface roughness on nanoindentation tests. *Procedia CIRP*, 8, pp. 334–339. https://doi.org/10.1016/j.procir.2013.06.112.

Chen, L., Ahadi, A., Zhou, J. and Ståhl, J., 2014. Numerical and experimental study of the roughness effects on mechanical properties of AISI316L by nanoindentation. *Modeling and Numerical Simulation of Material Science*, 4(4), pp. 153–162. http://dx.doi.org/10.4236/mnsms.2014.44017.

Deutsche Institut für Normung, 1993. *DIN EN 20187:1993-11 Papier, Pappe und Zellstoff; Normalklima für die Vorbehandlung und Prüfung und Verfahren zur Überwachung des Klimas und der Probenvorbehandlung (ISO 187:1990); Deutsche Fassung EN 20187:1993*. Berlin: DIN.

Deutsche Institut für Normung, 2018. *DIN 50014:2018-04 Normalklimate für Vorbehandlung und/oder Prüfung – Festlegungen*. Berlin: DIN.

Drexler, E., 2009. Nanostructures, nanomaterials, and lattice-scalled stiffness. *Metamodern: the trajectory of technology*, [blog] 15 February. Available at: <http://metamodern.com/2009/02/15/nanomaterials-nanostructures-and-stiffness/> [Accessed March 2020].

Endres, I., 2006. *Compression uniformity measurements on coated and uncoated paper surfaces*. Doctoral thesis. University of Karlstad.

Fujifilm, 2016. *Prescale Sheet Type*. [online] Fujifilm Corporation. Available at: <https://www.fujifilm.com/products/prescale/prescale_sheettype/> [Accessed March 2020].

Hansson, P. and Johansson, P.-Å., 2000. Topography and reflectance analysis of paper surfaces using a photometric stereo method. *Optical Engineering*, 39(9), pp. 2555–2561. https://doi.org/10.1117/1.1287261.

Kaulitz, T., 2009. *Bilden von Schneidlagen unter Ausnutzung des Nipinduzierten Effekts für die Druckweiterverarbeitung*. Doctoral dissertation. Technische Universität Darmstadt.

Kaulitz, T. and Dörsam, E., 2008. Highly accurate material characterization of paper for the simulation of printing process. In: N. Enlund and M. Lovreček, eds. *Advances in Printing and Media Technology: Proceeding of the 35th International Research Conference of iarigai*. Valencia, Spain, September 2008. Darmstadt, Germany, pp. 263–270.

Liu, B., Villavicencio, R. and Soares, C.G., 2013. Failure characteristics of strength-equivalent aluminium and steel plates in impact conditions. In: C. Guedes Soares and J. Romanoff, eds. *Analysis and Design of Marine Structures: Proceedings of the 4th International Conference on Marine Structures (MARSTRUCT 2013).* Espoo, Finland, 25–27 March 2013. Boca Raton, FL, USA: CRC Press, pp. 167–174.

Luong, C.H., 1999. *Experimental and theoretical investigations of mechanical and thermal relations by calendering of paper*. Doctoral thesis. Norwegian University of Science and Technology, Trondheim.

Mark, R.E., Haberger Jr., C.C., Borch, J. and Lyne, M.B. eds., 2001. *Handbook of physical testing of paper: Volume 1.* 2nd ed. Boca Raton, FL, USA: CRC Press.

MATLAB Help, 2013. *Image processing toolbox: user's guide – R2013b.* [pdf] MathWorks. Available at: <http://www.mathworks.com/downloads> [Accessed March 2020].

Otsu, N., 1979. A threshold selection method from gray-level histograms. *IEEE Transactions on Systems, Man and Cybernetics*, 9(1), pp. 62–66. https://doi.org/10.1109/TSMC.1979.4310076.

Pino, A. and Pladellorens, J., 2009. Measure of roughness of paper using speckle. In: P.S. Huang, T. Yoshizawa and K.G. Harding, eds. *Proceedings Vol. 7432: SPIE optical Engineering + Applications.* San Diego, CA, USA, 2–6 August 2009. SPIE, pp. 74320. https://doi.org/10.1117/12.825072.

Provatas, N. and Uesaka, T., 2003. Modelling paper structure and paper-press interactions, *Journal of Pulp and Paper Science*, 29(10), pp. 332–340.

Rättö, P., 2005. The influence of surface roughness on the compressive behaviour of paper, *Nordic Pulp and Paper Research Journal*, 20(3), pp. 304–307. https://doi.org/10.3183/npprj-2005-20-03-p304-307.

Schaffrath, H.-J. and Göttsching, L., 1991. The behavior of paper under compression in z-direction. In: *Proceedings of the 1991 Tappi International Paper Physics Conference.* Kona, HI, USA, 22–28 September 1991. Atlanta, USA: TAPPI Press, pp. 489–510.

Schaffrath, H.-J. and Göttsching, L., 1992a. Das Kompressionsverhalten von Papier in ZD. *Das Papier*, 46, pp. 74–81.

Schaffrath, H.-J. and Göttsching, L., 1992b. Modellierung der Kompression von Papier in z-Richtung bei niedriger Flächenpressung. *Das Papier*, 46(7), pp. 350–355.

Senden, D.J.A., 2013. *Strain hardening and anisotropy in solid polymers*. Doctoral thesis. Technische Universiteit Eindhoven.

Singh, S.P., 2008. A comparison of different methods of paper surface smoothness evaluation. *BioResources,* 3(2), pp. 503–516.

Stenberg, N., 2003. A model for the through-thickness elastic-plastic behaviour of paper. *International Journal of Solids and Structures,* 40(26), pp. 7483–7498. https://doi.org/10.1016/j.ijsolstr.2003.09.003.

Teleman, A., Östlund, C., Nordström, J.-E., Johansson, P.-Å. and Vomhoff, H., 2004. *Analysis of paper surface topography under compression: STFI report CW217*. Stockholm, Sweden: STFI.

Turner, C.H. and Burr, D.B., 1993. Basic biomechanical measurements of bone: a tutorial. *Bone*, 14(4), pp. 595–608. https://doi.org/10.1016/8756-3282(93)90081-K.

Vernhes, P., Bloch, J.-F., Blayo, A. and Pineaux, B., 2009. Effect of calendering on paper surface micro-structure: a multi-scale analysis. *Journal of Materials Processing Technology*, 209(11), pp. 5204–5210. https://doi.org/10.1016/j.jmatprotec.2009.03.005.

Vernhes, P., Dubé, M. and Bloch, J.-F., 2010. Effect of calendering on paper surface properties. *Applied Surface Science*, 256(22), pp. 6923–6927. https://doi.org/10.1016/j.apsusc.2010.05.004.

Xia, Q.S., Boyce, M.C. and Parks, D.M., 2002. A constitutive model for the anisotropic elastic-plastic deformation of paper and paperboard. *International Journal of Solids and Structures,* 39(15), pp. 4053–4071. https://doi.org/10.1016/S0020-7683(02)00238-X.

Yuce, C., Karpat, F., Yavuz, N. and Sendeniz, G., 2014. A Case study: designing for sustainability and reliability in an automotive seat structure. *Sustainability*, 6(7), pp. 4608–4631. https://doi.org/10.3390/su6074608.